Chapter 2

Experimental Aspects of Polarization Optimized Experiments (POE) for Magic Angle Spinning Solid-State NMR of Microcrystalline and Membrane-Bound Proteins

T. Gopinath and Gianluigi Veglia

Abstract

Conventional NMR pulse sequences record one spectrum per experiment, while spending most of the time waiting for the spin system to return to the equilibrium. As a result, a full set of multidimensional NMR experiments for biological macromolecules may take up to several months to complete. Here, we present a practical guide for setting up a new class of MAS solid-state NMR experiments (POE or polarization optimized experiments) that enable the simultaneous acquisition of multiple spectra of proteins, accelerating data acquisition. POE exploit the long-lived ^{15}N polarization of isotopically labeled proteins and enable one to obtain up to eight spectra, by concatenating classical NMR pulse sequences. This new strategy propels data throughput of solid-state NMR spectroscopy of fibers, microcrystalline preparations, as well as membrane proteins.

Key words Solid-state NMR, Multiple acquisitions, POE, DUMAS, MEIOSIS, MAeSTOSO, SIM-CP

1 Introduction

Magic angle spinning solid-state NMR (MAS ssNMR) spectroscopy plays a central role in the characterization of structure, motions, and interactions of biological macromolecules [1–6]. Unlike X-ray crystallography, MAS ssNMR does not require well-diffracting crystals and is able to analyze protein fibrils, microcrystalline preparations, as well as membrane proteins in their natural lipid environments [7–11]. However, the low-throughput of ssNMR data is a significant concern. As a result, the number of protein structures or dynamic studies utilizing ssNMR is rather sparse.

A significant hurdle is the intrinsic low sensitivity of NMR spectroscopy, which makes data acquisition time-consuming. NMR researchers must invest a significant portion of time and budgetary resources to carry out several multidimensional NMR

Ranajeet Ghose (ed.), *Protein NMR: Methods and Protocols*, Methods in Molecular Biology, vol. 1688,
DOI 10.1007/978-1-4939-7386-6_2, © Springer Science+Business Media LLC 2018

experiments for resonance assignments and structure determination. Recent developments in both software and hardware have alleviated these problems to a large extent. Technical developments include higher static magnetic fields (B_o), low-E or E-free probes that increase the sensitivity of the RF coil, avoiding heating caused by high-power decoupling pulses [12–14], dynamic nuclear polarization (DNP) [15], paramagnetic relaxation enhancement (PRE) [16], as well as the most recent ^{1}H detection methods using fast and ultra-fast MAS probes [17–19].

We recently introduced a new class of experiments, called POE for polarization optimized experiments, which are based on long-lived ^{15}N polarization generated for biological solids that enable the acquisition of multiple discrete NMR spectra simultaneously [20–24]. POE are synergistic to the above methods and promise to speed up the acquisition of solid-state NMR data. Specifically, POE are based on the detection of multiple FIDs from orphan polarization that is discarded in classical ssNMR experiments. The development of POE was inspired by the work of Alex Pines, who noted that multiple cross-polarization experiments enable one to record several FIDs sequentially [25]. Along these lines, the "afterglow" effects of polarization have been previously introduced for both solution and solid-state NMR experiments for acquiring multiple spectra simultaneously [26–28]. Unlike solution NMR experiments, where the T_1 relaxation is quite rapid, solid-state NMR experiments can be designed in a way that ^{15}N polarization originating from a simultaneous cross-polarization scheme (SIM-CP) can be stored along the z-direction and exploited for multiple experiments using a single pulse sequence.

In this paper, we provide a step-by-step guide to the design and concatenation of several multidimensional MAS ssNMR experiments to optimize the time on the NMR spectrometers. We will describe our recent pulse schemes, DUMAS, MEIOSIS, and MAeSTOSO with a detailed description of experimental setup, data acquisition, and processing.

2 POE: A New Class of Experiments for Simultaneous Acquisition of ssNMR Spectra

Solid-state NMR experiments utilize about 5–10% of the total experimental time for pulse execution and acquisition of the signal (FID), while for 90–95% of the time the spectrometer is idle (2–3 s) waiting for the spin system to return to the equilibrium (i.e., through longitudinal relaxation, T_1) and to conform to probe duty cycle guidelines. Classical ssNMR methods are designed for a single acquisition period, where each 2D or 3D experiment is acquired separately from the evolution, coherence transfer, and detection of a specific polarization pathway. The basic ideas behind POE include (1) the creation of multiple spin polarization

pathways, and (2) the acquisition of multiple 2D experiments using two to four acquisition periods per each scan. Using these two concepts, we are able to concatenate several different experiments and obtain multiple spectra using a single pulse sequence. Specifically, we have developed four different strategies for POE (Fig. 1). Our most recent implementation, MAeSTOSO-8, makes it possible to acquire up to eight different experiments simultaneously. In principle, there are multiple combinations possible for each of these experiments. A few examples are reported in Fig. 2.

The central element in each of these methods is the simultaneous cross-polarization (SIM-CP) that creates two polarization pathways for ^{13}C and ^{15}N. For instance, in the DUMAS experiment, ^{13}C and ^{15}N polarization originating from SIM-CP is used to acquire the CXCX and NCA experiments in the first and second acquisition periods, respectively (Fig. 2a). A similar scheme is used in MAeSTOSO-4, where CXCX and NCACB are acquired in the first and second acquisitions, and two more experiments (NCACX and NCO) can be also acquired utilizing the residual ^{15}N polarization resulting from the NC transfer periods. MEIOSIS, on the other hand, was designed to concatenate C(N)C with CC and NC correlation experiments using two acquisitions per scan. In the MEIOSIS experiment (Fig. 2c), CXCX and NCACX are acquired in first acquisition, whereas CA(N)CO and NCO are recorded in the second acquisition period. To deconvolute the two polarization pathways, two data sets with alternating ϕ phases (x and –x) of ^{15}N spin-lock are recorded. Using similar strategies, the simultaneous acquisition of up to eight FIDs (MAeSTOSO-8) can be achieved with four acquisition periods (Fig. 2d).

3 Experimental Setup of POE and Data Acquisition

Modern MAS ssNMR experiments on proteins are generally carried out using either fast spinning speeds with 1.3 mm diameter rotors or moderate spinning speeds with 3.2 mm rotors. The typical sample volume for a 1.3 mm rotor is about 3 μL, reaching high spinning speeds (~40–60 kHz) that truncate the ^{1}H–^{1}H dipolar coupling network and enabling ^{1}H detection for high sensitivity [17, 29, 30]. Due to the small volume, the 1.3 mm probes and rotors are mainly used for highly concentrated protein samples such as microcrystalline preparations with low hydration levels. In contrast, the MAS probes with 3.2 mm rotors can accommodate up to 30 μL sample with maximum spinning speed of approximately 10–15 kHz. Due to the larger sample volume, these rotors can accommodate fully hydrated samples such as membrane proteins, whose concentrations are quite dilute due to the presence of lipids necessary to maintain their native state. Under these moderate spinning speed conditions, ^{1}H resonances are very broad, and

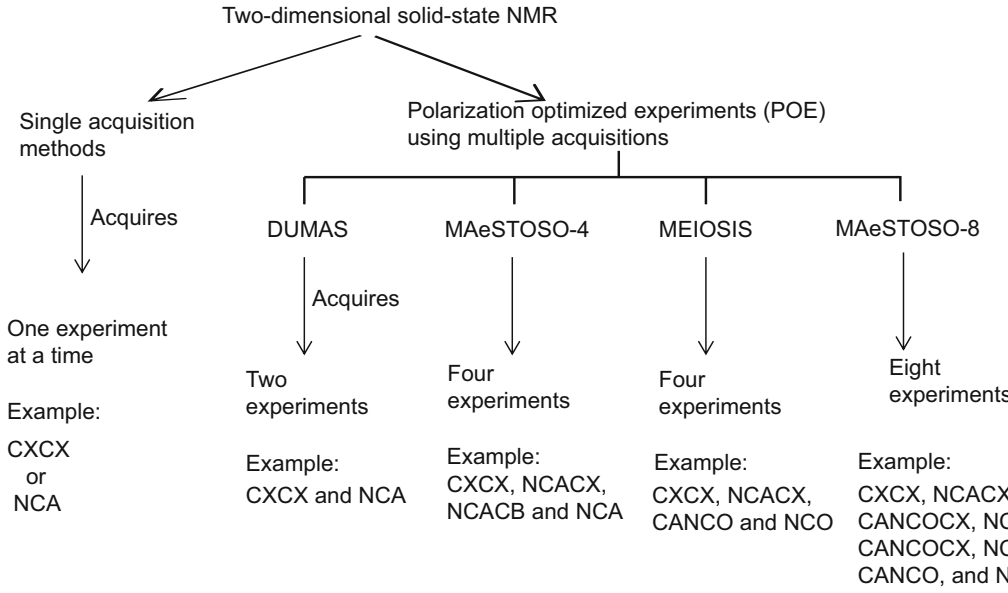


Fig. 1 Schematic of two-dimensional ssNMR methodologies. Conventional single-acquisition methods record one experiment at a time. POE class of experiments enable the acquisition of multiple 2D spectra using DUMAS, MAeSTOSO-4, MEIOSIS, and MAeSTOSO-8 strategies

spectroscopic studies are usually carried out using ^{13}C-detected multidimensional experiments. Indeed, POE are most effective for membrane protein samples under moderate spinning speed conditions and with 3.2 mm or 4 mm MAS probes.

To demonstrate the performance of the POE methods, we utilized a microcrystalline preparation with U-^{13}C,^{15}N labeled ubiquitin and two U-^{13}C,^{15}N labeled membrane proteins (phospholamban, PLN, and sarcolipin, SLN) as benchmarks. The microcrystalline U-^{13}C,^{15}N ubiquitin sample consisted of ~8 mg of protein, whereas PLN and SLN were reconstituted in 1,2-dimyristoyl-sn-glycero-3-phosphocholine (DMPC) lipids to an approximate 1:100 protein-to-lipid ratio using our standard protocols [3, 24, 31]. Note that our membrane protein preparations contain at least 100 lipids per protein to maintain native-like conditions and avoid aggregations. Typically, the reconstituted samples contain 2–3 mg of protein and 15 mg of DMPC lipids. After organic solvent- or detergent-mediated reconstitution, the lipoproteins are centrifuged and the pellets with approximately 30% (w/v) hydration level are packed into 3.2 mm rotors for spectral analysis.

POE have been implemented on 600 MHz Agilent spectrometers using 3.2 mm scroll coil MAS probe. All of the relevant experimental parameters are summarized in Table 1. For hydrated samples such as membrane proteins, the sample temperature plays a major role for optimal sensitivity and resolution. For proteoliposomes, the sample temperature can affect the lipid phase and

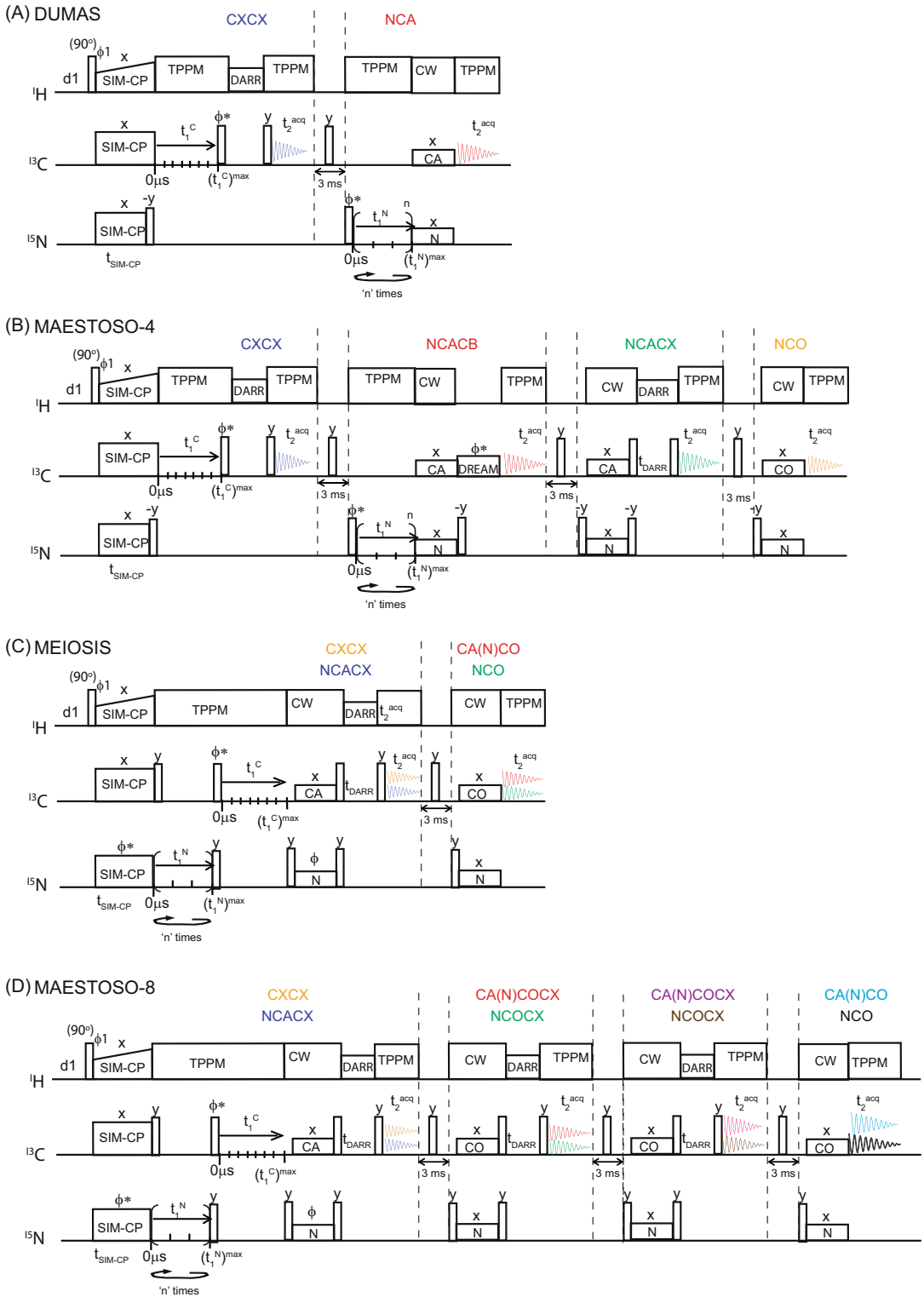


Fig. 2 Concatenation of 2D ssNMR experiments using DUMAS, MAeSTOSO-4, MEIOSIS, and MAeSTOSO-8

Table 1
Experimental parameters used for the POE experiments reported in Fig. 2

Parameter	Value	Parameter	Value	Parameter	Value
d1(Recycle delay)	2 s	t_{2acq}	15–20 ms	Dwell time of t_1^c	30 μs
MAS rate	12 kHz	Dwell time of t2	10 μs	Number of t_1^c increments	256
$A^H_{SIM\text{-}CP}$	59 kHz	A^H_{TPPM}	100 kHz	$(t_1^C)^{max}$	7680 μs
$A^C_{SIM\text{-}CP}$	35 kHz	^{1}H offset	5 ppm	Dwell time of $t^1{}_N$	300 μs
$A^N_{SIM\text{-}CP}$	35 kHz	^{15}N offset	120 ppm	Number of t_1^N increments	32
$\Delta^H_{SIM\text{-}CP}$	2 kHz	^{15}C offset	100 ppm	$(t_1^N)^{max}$	9600 μs
$t_{SIM\text{-}CP}$	300–1000 μs			Number of $t^1{}_N$ loops	8
90° pulses					
$A^H{}_{90}$	100 kHz	$A^C{}_{90}$	41.6 kHz	$A^N{}_{90}$	41.6 kHz
$t^H{}_{90}$	2.5 μs	$t^C{}_{90}$	6 μs	$t^N{}_{90}$	6 μs
CC mixing				NC mixing	
CXCX		CACB		NCA/NCO	
^{13}C offset	100 ppm	^{13}C offset	52 ppm	^{13}C offset (NCA)	55 ppm
t_{DARR}	20–500 ms	t_{DREAM}	2.53 ms	A^C (NCA)	18.5 kHz
$A^H{}_{DARR}$	12 kHz	$A^H{}_{DREAM}$ $\Delta^C{}_{DREAM}$ $\beta^C{}_{DREAM}$	6.69 kHz 3.12 kHz 1.56 kHz	^{13}C offset (NCO) A^C (NCO) ^{15}N offset (NCA/NCO) A^N (NCA/NCO) Δ^C (NCA/NCO) β^C (NCA/NCO) $t_{NCA/NCO}$	170 ppm 39.8 kHz 120 ppm 31 kHz 2.8 kHz 0.9 kHz 3 ms

$X^N{}_P$: RF amplitude of "X" applied on nucleus "N" during the pulse sequence block "P"; t_p: Time period "t" of the pulse sequence block "p"

protein's rotational diffusion, influencing both sensitivity and resolution. At 25 °C, DMPC lipids are in the liquid crystalline phase, which promotes the protein's rotational diffusion, which scales dipolar couplings (DC) and lowers the performance of the cross-polarization. On the other hand, protein spectra recorded at 0–4 °C with the lipids in gel phase are more sensitive. In addition to temperature, sensitivity changes are also dictated by the protein size, lipid composition, and protein-lipid interactions. Although it is always preferable to carry out the NMR experiments under conditions close to the liquid crystalline phase, the lower sensitivity may represent a serious hurdle, extending the experimental acquisition time significantly.

For all POE reported in Figs. 1 and 2, and Table 1, the recycle delay was set to 2 s, and MAS rate (ω_r) to 12 kHz. As per probe requirements, the maximum RF amplitude on the ^{1}H channel was set to 100 kHz, which corresponds to a 2.5 μs 90° pulse; whereas for ^{13}C and ^{15}N a 6 μs 90° pulses were used, corresponding to 41.6 kHz RF amplitude. During the t_1 evolution and t_2 acquisition periods, a TPPM decoupling sequence was used on the ^{1}H channel with a 100 kHz RF amplitude [32]. During SIM-CP, the RF amplitudes for ^{13}C and ^{15}N were set to 35 kHz, and ^{1}H RF amplitude was ramped, with the center of ramp set to 59 kHz satisfying the Hartman-Hahn matching condition at 12 kHz MAS rate [33]. Typical contact times for SIM-CP range from 300 to 1000 μs. Usually, the backbone $^{15}N^{H}$ and ^{13}CH groups are cross-polarized at contact times ranging from 300 to 500 μs, whereas ^{13}CO, $^{13}CH_2$, and NH_2 groups require longer contact times up to 1000–1500 μs. In our experiments, we generally set SIM-CP contact time at 500 μs to obtain maximum intensity for ^{13}Cα, and $^{15}N^{H}$ nuclei of the protein backbone. Note that optimal contact times can vary significantly among different samples depending on the hydration levels.

Specific CP that transfers polarization between ^{13}C and ^{15}N nuclei is another important building block for classical triple-resonance MAS ssNMR experiments as well as for POE. Unlike for ^{1}H-^{13}C and ^{1}H-^{15}N polarization transfer via CP or SIM-CP, the NC transfer is mediated by relatively weak DC between ^{13}C and ^{15}N, and thus requires careful optimization of specific-CP RF parameters [34, 35]. In other words, the rotating frame matching condition for NC transfer is relatively narrow compared to HC or HN CP transfer. In our case NC transfer was obtained by using tangent-shaped ramp pulse on ^{13}C and constant amplitude pulse was applied on ^{15}N, while applying a 100 kHz RF for ^{1}H decoupling. Theoretical RF amplitudes for the NCA transfer are $1.5\omega_r$ and $2.5\omega_r$ for ^{13}C, ^{15}N, respectively, where ω_r is the spinning rate. For the NCO transfer, the theoretical values are $3.5\omega_r$ and $2.5\omega_r$ for ^{13}C and ^{15}N, respectively. Note that the optimal experimental RF values for NC transfer slightly deviate from the theoretical ones (Table 1). Typically, one needs to optimize these values, starting from the theoretical values and arraying the acquisition of multiple 1D experiments to select the best parameters for the highest sensitivity. We typically carry out this optimization acquiring the 1st increment of the 2D DUMAS experiments, where the second acquisition used to optimize the RF parameters for the NC transfer including the tangential ^{13}C ramp parameters Δ and β. Similarly, we optimize the DREAM mixing period for the CACB transfer using the second acquisition of MAeSTOSO-4 [36]. For the CXCX experiments, the DARR mixing times are based on the desired intra- or inter-residue correlations [37]. Typical DARR mixing times are in the range of 20–500 ms. Note that longer mixing

times cause a reduction in the overall sensitivity of the experiment and require more scans.

The t_2 acquisition times (t_{2acq}) for DUMAS and MEIOSIS are usually set to 20 ms, whereas for MAeSTOSO experiments t_{2acq} are set to 15 ms to avoid RF heating. While all t_{2acq} on ^{13}C use identical parameters, the indirect t_1 evolution times for ^{13}C and ^{15}N (t_{1c} and t_{1N}) must be synchronized. Usually, the ^{15}N evolution requires fewer t_1 increments than ^{13}C due to the longer dwell times. For example, a t_1 dwell time of 30 μs and 256 increments covers a ^{13}C spectral width of 33.33 kHz with a total t_1 evolution time of 7.68 ms. In contrast, the ^{15}N evolution requires a 300 μs dwell time with only 32 increments for a total t_1 evolution period of 9.6 ms. In order to synchronize the 256 increments of ^{13}C evolution with the ^{15}N evolution periods, each of the 32 increments for the ^{15}N evolution is repeated eight times (number of loops in Table 1) and added in the spectral processing. As a result, the effective number of scans for the processed NC spectra will be eight times higher compared to the CC correlation spectra. All the data sets are externally referenced to the CH_2 resonance of adamantane at 40.48 ppm and processed using NMRPipe as described below [38].

4 Processing POE Experiments

POE require special data processing to deconvolute the individual FID data sets and then Fourier transform them into multiple 2D spectra. Figure 3 shows the layout of the processing procedure using NMRpipe scripts [38]. Briefly, the raw data are first converted into multiple 2D FID data sets by executing *fid.com* script that contains the experimental acquisition parameters. The *fid.com* scripts for DUMAS and MAeSTOSO-4 are reported in Table 2, while the *fid.com* for MEIOSIS and MAeSTOSO-8 are shown in Table 3. For all four experiments (DUMAS, MAeSTOSO, MEIOSIS, and MAERSTOSO-8) the numbers of t_1 complex points for ^{13}C and ^{15}N evolution are set to 256 and 32, respectively, with eight loops for ^{15}N t_1 evolution. Note that in the *fid.com* script for conventional 2D experiments (one acquisition per scan) the "yN" and "yT" variables correspond to real and complex points, respectively. In the POE data sets, however, the definitions of yN and yT are given in Table 4. Depending on the experimental scheme, the outputs from the *fid.com* input file generate one to four ^{13}C- and ^{15}N-edited time domains in the 2D data sets. For instance, in the DUMAS experiment, the *fid.com* input file deconvolutes the FID into two data sets, CC.fid and NC.fid, which correspond to ^{13}C- and ^{15}N-edited experiments acquired in the first and second acquisition periods. On the other hand, in the MAeSTOSO-8-experiment, the ^{13}C-edited 2D data sets (CC.fid, CNC1.fid,

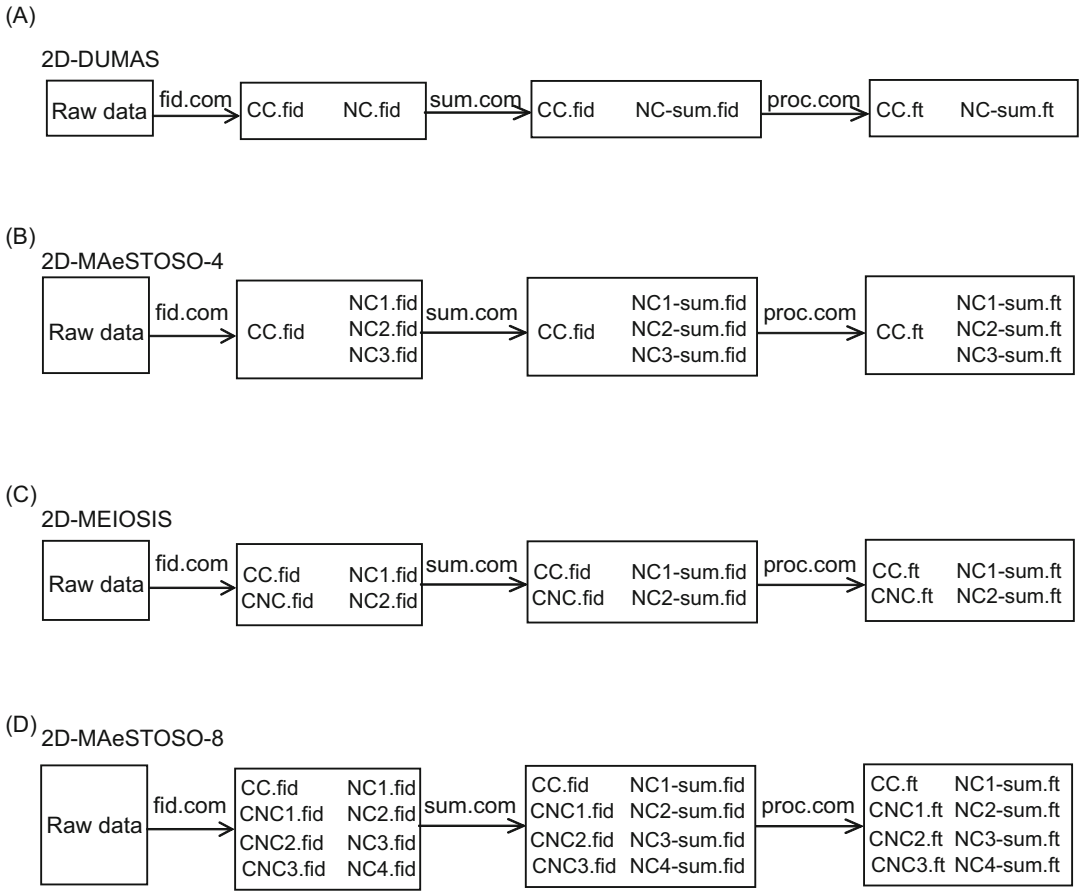


Fig. 3 Data processing procedure of 2D ssNMR data acquired from DUMAS, MAeSTOSO-4, MEIOSIS, and MAeSTOSO-8 experiments. NMRpipe scripts for fid.com, sum.com, and proc.com are given in Tables 2–6

CNC2.fid, and CNC3.fid) are deconvoluted from the FID (test.fid) using the COADD command line in the *fid.com* script. Similarly, the ^{15}N-edited 2D data sets (NC.fid, NC1.fid, NC2.fid, and NC3.fid) are deconvoluted from the test1.fid file. Following this step, the ^{13}C-edited data sets remain the same, whereas each of the ^{15}N-edited 2D data sets is further separated into eight t_1 data sets ($n = 8$ loops) and then corresponding t_1 increments in each of the eight data sets is added using the *sum.com* script as shown in Table 5. In the final step, multiple 2D spectra are generated by 2D Fourier transformation executing the *proc.com* script (Table 6) on each of the ^{13}C- and ^{15}N- edited 2D data sets. Figure 4 shows the 2D DUMAS spectra of sarcolipin membrane protein, and

Table 2
NMRpipe script for DUMAS and MAeSTOSO-4 for converting the raw data into nmrpipe format

#2D DUMAS 'fid.com' script
#Number of 13C t1 complex points=256
#Number of 15N t1 complex points=32
#Number of 15N t1 loops=8

varAdjust -in fid -out fid.adj -ov
var2pipe -in fid.adj -noaswap -pw 0 \
-xN 4000 -yN 1024 \
-xT 2000 -yT 256 \
-xMODE Complex -yMODE complex \
-xSW 100000.000 -ySW 33333.33 \
-xOBS 150.787 -yOBS 150.787 \
-xCAR 100.0 -yCAR 100.0 \
-xLAB C13 -yLAB C13 \
-ndim 2 -aq2D Real \
-out ./test.fid -verb -ov

nmrPipe -in test.fid \
| nmrPipe -fn COADD -axis Y -cList 1 0 -time \
-verb -ov -out **CC.fid**

varAdjust -in fid -out fid.adj -ov
var2pipe -in fid.adj -noaswap -pw 0 \
-xN 4000 -yN 1024 \
-xT 2000 -yT 256 \
-xMODE Complex -yMODE complex \
-xSW 100000.000 -ySW 3333.33\
-xOBS 150.787 -yOBS 60.766 \
-xCAR 96.87 -yCAR 118.74 \
-xLAB C13 -yLAB N15 \
-ndim 2 -aq2D Real \
-out ./test1.fid -verb –ov

nmrPipe -in test1.fid \
| nmrPipe -fn COADD -axis Y -cList 0 1 -time \
-verb -ov -out **NC.fid**

#2D MAeSTOSO-4 'fid.com' script
#Number of 13C t1 complex points=256
#Number of 15N t1 complex points=32
#Number of 15N t1 loops=8

varAdjust -in fid -out fid.adj -ov
var2pipe -in fid.adj -noaswap -pw 0 \
-xN 4000 -yN 2048 \
-xT 2000 -yT 256 \
-xMODE Complex -yMODE complex \
-xSW 100000.000 -ySW 33333.33 \
-xOBS 150.787 -yOBS 150.787 \
-xCAR 100.0 -yCAR 100.0 \
-xLAB C13 -yLAB C13 \
-ndim 2 -aq2D Real \
-out ./test.fid -verb -ov

nmrPipe -in test.fid \
| nmrPipe -fn COADD -axis Y -cList 1 0 0 0-time \
-verb -ov -out **CC.fid**

varAdjust -in fid -out fid.adj -ov
var2pipe -in fid.adj -noaswap -pw 0 \
-xN 4000 -yN 1024 \
-xT 2000 -yT 256 \
-xMODE Complex -yMODE complex \
-xSW 100000.000 -ySW 3333.33\
-xOBS 150.787 -yOBS 60.766 \
-xCAR 96.87 -yCAR 118.74 \
-xLAB C13 -yLAB N15 \
-ndim 2 -aq2D Real \
-out ./test1.fid -verb –ov

nmrPipe -in test1.fid \
| nmrPipe -fn COADD -axis Y -cList 0 1 0 0 -time \
-verb -ov -out **NC1.fid**
nmrPipe -in test1.fid \
| nmrPipe -fn COADD -axis Y -cList 0 0 1 0 -time \
-verb -ov -out **NC2.fid**
nmrPipe -in test1.fid \
| nmrPipe -fn COADD -axis Y -cList 0 0 1 0 -time \
-verb -ov -out **NC3.fid**
nmrPipe -in test1.fid \
| nmrPipe -fn COADD -axis Y -cList 0 0 0 1 -time \
-verb -ov -out **NC4.fid**

MAeSTOSO-4 spectra of ubiquitin microscrystalline preparation using the acquisition parameters shown in Table 1. The spectra were processed using the *fid.com* (Table 2), *sum.com* (Table 5), *proc.com* (Table 6) scripts in NMRpipe.

Table 3
NMRpipe script for MEIOSIS and MeESTOSO-8 for converting the raw data into nmrpipe format

```
#2D MEIOSIS 'fid.com' script
#Number of 13C t1 complex points=256
#Number of 15N t1 complex points=32
#Number of 15N t1 loops=8


varAdjust -in fid -out fid.adj -ov
var2pipe -in fid.adj -noaswap -pw 0 \
 -xN            4000  -yN             2048  \
 -xT            2000  -yT              512  \
 -xMODE       Complex  -yMODE        complex  \
 -xSW      100000.000  -ySW         33333.33  \
 -xOBS        150.787  -yOBS         150.787  \
 -xCAR          100.0  -yCAR           100.0  \
 -xLAB            C13  -yLAB             C13  \
 -ndim              2  -aq2D          Real  \
 -out ./test.fid -verb -ov

nmrPipe -in test.fid \
| nmrPipe  -fn COADD -axis Y -cList 1 0 1 0 -time \
-verb -ov -out CC.fid
nmrPipe -in test.fid \
| nmrPipe  -fn COADD -axis Y -cList 0 1 0 1 -time \
-verb -ov -out CNC.fid


varAdjust -in fid -out fid.adj -ov
var2pipe -in fid.adj -noaswap -pw 0 \
 -xN            4000  -yN             2048  \
 -xT            2000  -yT              256  \
 -xMODE       Complex  -yMODE        complex  \
 -xSW      100000.000  -ySW          3333.33\
 -xOBS        150.787  -yOBS         60.766  \
 -xCAR          96.87  -yCAR          118.74  \
 -xLAB            C13  -yLAB             N15  \
 -ndim              2  -aq2D          Real  \
 -out ./test1.fid -verb –ov

nmrPipe -in test1.fid \
| nmrPipe  -fn COADD -axis Y -cList 1 0 -1 0 -time \
-verb -ov -out NC1.fid
nmrPipe -in test1.fid \
| nmrPipe  -fn COADD -axis Y -cList 0 1 0 -1 -time \
-verb -ov -out NC2.fid
```

```
#2D MAeSTOSO-8 'fid.com' script
#Number of 13C t1 complex points=256
#Number of 15N t1 complex points=32
#Number of 15N t1 loops=8


varAdjust -in fid -out fid.adj -ov
var2pipe -in fid.adj -noaswap -pw 0 \
 -xN            4000  -yN             4096 \
 -xT            2000  -yT             1024  \
 -xMODE       Complex  -yMODE        complex  \
 -xSW      100000.000  -ySW         33333.33  \
 -xOBS        150.787  -yOBS         150.787  \
 -xCAR          100.0  -yCAR           100.0  \
 -xLAB            C13  -yLAB             C13  \
 -ndim              2  -aq2D          Real  \
 -out ./test.fid -verb -ov

nmrPipe -in test.fid \
| nmrPipe  -fn COADD -axis Y -cList 1 0 0 0 1 0 0 0 -time \
-verb -ov -out CC.fid
nmrPipe -in test.fid \
| nmrPipe  -fn COADD -axis Y -cList 0 1 0 0 0 1 0 0 -time \
-verb -ov -out CNC1.fid
nmrPipe -in test.fid \
| nmrPipe  -fn COADD -axis Y -cList 0 0 1 0 0 0 1 0 -time \
-verb -ov -out CNC2.fid
nmrPipe -in test.fid \
| nmrPipe  -fn COADD -axis Y -cList 0 0 0 1 0 0 0 1 -time \
-verb -ov -out CNC3.fid


varAdjust -in fid -out fid.adj -ov
var2pipe -in fid.adj -noaswap -pw 0 \
 -xN            4000  -yN             4096  \
 -xT            2000  -yT              256  \
 -xMODE       Complex  -yMODE        complex  \
 -xSW      100000.000  -ySW          3333.33\
 -xOBS        150.787  -yOBS         60.766  \
 -xCAR          96.87  -yCAR          118.74  \
 -xLAB            C13  -yLAB             N15  \
 -ndim              2  -aq2D          Real  \
 -out ./test1.fid -verb –ov

nmrPipe -in test1.fid \
| nmrPipe  -fn COADD -axis Y -cList 1 0 0 0 -1 0 0 0 -time \
-verb -ov -out NC1.fid
nmrPipe -in test.fid \
| nmrPipe  -fn COADD -axis Y -cList 0 1 0 0 0 -1 0 0 -time \
-verb -ov -out NC2.fid
nmrPipe -in test.fid \
| nmrPipe  -fn COADD -axis Y -cList 0 0 1 0 0 0 -1 0 -time \
-verb -ov -out NC3.fid
nmrPipe -in test.fid \
| nmrPipe  -fn COADD -axis Y -cList 0 0 0 1 0 0 0 -1 -time \
-verb -ov -out NC3.fid
```

Table 4
Definition of "yN" and "yT" used in fid.com script of Table 2

POE scheme	No. of FIDs per scan (nf)	No. of polarization pathways per FID (np)	Total no. of 2D experiments combined (nf*np)	No. of complex points (nc)	No. of t1 loops (n)	yN = 2nf*np*nc*n	yT
DUMAS	2	1	2	256 (for ^{13}C) 32 (for ^{15}N)	1 (for ^{13}C) 8 (for ^{15}N)	1024	256
MAeSTOSO-4	4	1	4	256 (for ^{13}C) 32 (for ^{15}N)	1 (for ^{13}C) 8 (for ^{15}N)	2048	256
MEIOSIS	2	2	4	256 (for ^{13}C) 32 (for ^{15}N)	1 (for ^{13}C) 8 (for ^{15}N)	2048	512
MAeSTOSO-8	4	2	8	256 (for ^{13}C) 32 (for ^{15}N)	1 (for ^{13}C) 8 (for ^{15}N)	4096	1024

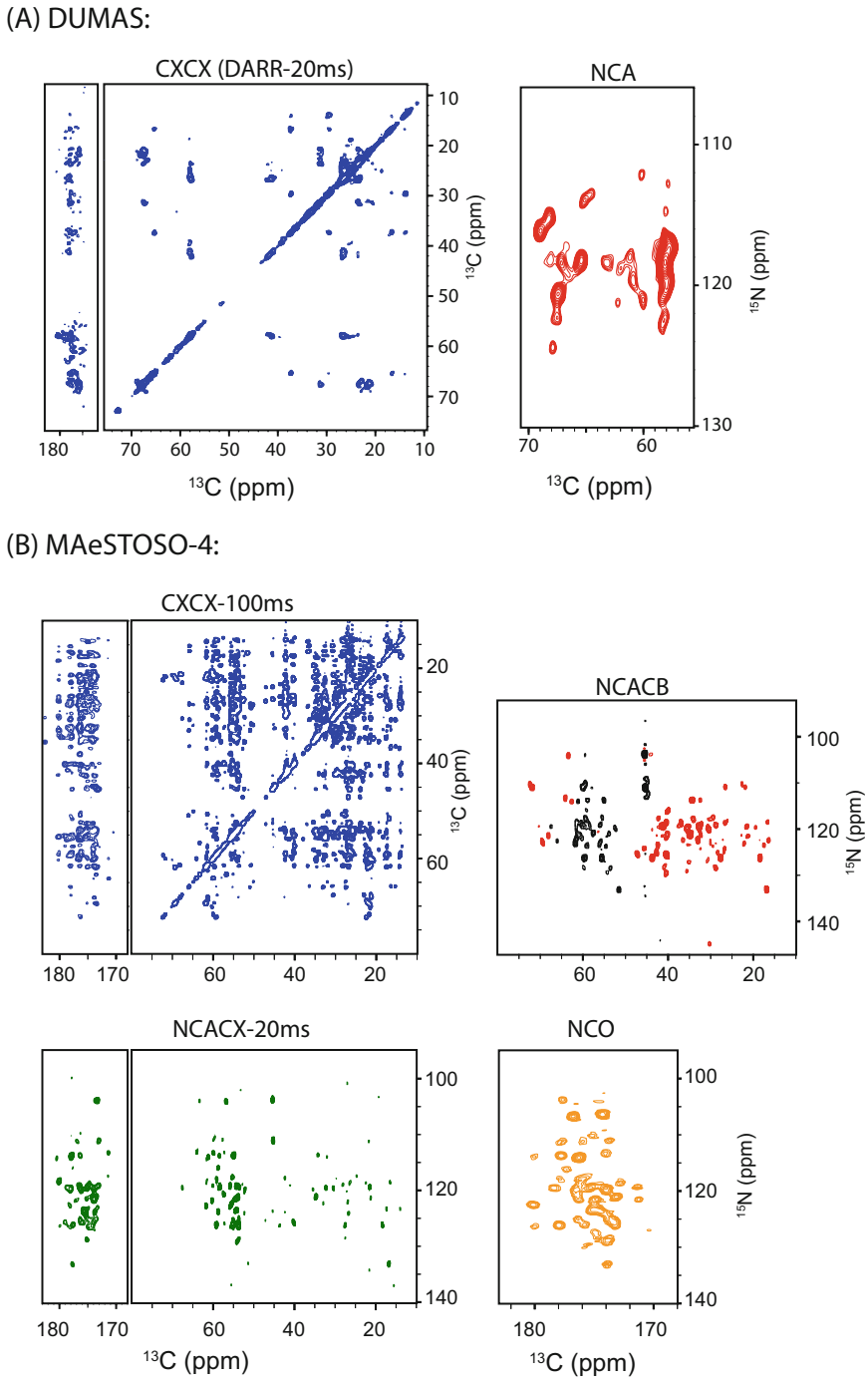


Fig. 4 (**a**) CXCX and NCA spectra of sarcolipin membrane protein acquired using 2D DUMAS pulse sequence of Fig. 2a. (**b**) Application of MAeSTOSO-4 (Fig. 2b) for Simultaneous acquisition of CXCX, NCACB, NCACX, and NCO spectra of ubiquitin microcrystalline protein

Table 5
NMRpipe script for adding the sub 2D data sets of NC.fid

#sum.com script

```
nmrPipe -in NC.fid \
| nmrPipe  -fn EXT -yn 64 -y1 1 -verb \
  -verb -ov -out 1.fid

nmrPipe -in NC.fid \
| nmrPipe  -fn EXT -yn 128 -y1 65 -verb \
  -verb -ov -out 2.fid

nmrPipe -in NC.fid \
| nmrPipe  -fn EXT -yn 192 -y1 129 -verb \
  -verb -ov -out 3.fid

nmrPipe -in NC.fid \
| nmrPipe  -fn EXT -yn 256 -y1 193  -verb \
  -verb -ov -out 4.fid

nmrPipe -in NC.fid \
| nmrPipe  -fn EXT -yn 320 -y1 257 -verb \
  -verb -ov -out 5.fid

nmrPipe -in NC.fid \
| nmrPipe  -fn EXT -yn 384 -y1 321 -verb \
  -verb -ov -out 6.fid

nmrPipe -in NC.fid \
| nmrPipe  -fn EXT -yn 448 -y1 385 -verb \
  -verb -ov -out 7.fid

nmrPipe -in NC.fid \
| nmrPipe  -fn EXT -yn 512 -y1 449  -verb \
  -verb -ov -out 8.fid
```

```
addNMR -in1 1.fid -in2 2.fid -out 12.fid -add
addNMR -in1 3.fid -in2 4.fid -out 34.fid -add
addNMR -in1 5.fid -in2 6.fid -out 56.fid -add
addNMR -in1 7.fid -in2 8.fid -out 78.fid -add
addNMR -in1 12.fid -in2 34.fid -out 1234.fid -add
addNMR -in1 56.fid -in2 78.fid -out 5678.fid -add
addNMR -in1 1234.fid -in2 5678.fid -out NC.fid -add

rm –r 1.fid 2.fid 3.fid 4.fid 5.fid 6.fid 7.fid 8.fid
rm –r 1234.fid 5678.fid
```

Table 6
NMRpipe script for 2D Fourier transformation

```
#proc.com script
#!/bin/csh

nmrPipe -in CC.fid \
| nmrPipe  -fn GM -g1 80 -g2 120    \
| nmrPipe  -fn ZF -size 16000              \
| nmrPipe  -fn FT                          \
| nmrPipe  -fn PS -p0 0.0 -p1.0 -di  \
| nmrPipe  -fn EXT -x1 0ppm -xn 200ppm -sw \
| nmrPipe  -fn TP                           \
| nmrPipe  -fn ZF -size 1024                \
| nmrPipe  -fn FT                          \
| nmrPipe  -fn PS -p0 0.0 -p1 0.0  -di \
| nmrPipe  -fn EXT -x1 0ppm -xn 80ppm -sw \
| nmrPipe  -fn TP                           \
| nmrPipe  -fn POLY -auto                   \
  -verb -ov -out cc.ft
```

5 Conclusions

POE presented in this chapter integrate various NMR pulse sequences using state-of-art NMR probe technology. This new class of experiments is not an alternative to the existing approaches to speed up data acquisition and increase sensitivity; rather it provides a clever strategy to concatenate multiple experiments into a single pulse sequence to optimize the timing of the spectrometers and speed up data acquisition through the acquisition of multiple 2D and 3D experiments. Utilizing POE-based strategies, for our proteins, we observed a reduction of approximately 50% of the experimental time compared to acquiring the corresponding experiments individually in a serial fashion. POE represent a general strategy for multiple acquisitions of almost all types of double- and triple-resonance ^{13}C detected experiments. When applied in concert with other fast acquisition and sensitivity enhancement techniques (e.g., Dynamic Nuclear Polarization, Paramagnetic Relaxation Enhancements, etc.), this approach can further push the boundaries of ssNMR applications to structural biology.

Acknowledgments

This research is supported by the National Institute of Health (GM 64742 and GM 72701 to G. V.). All of the NMR Experiments were carried out at the Minnesota NMR Center.

References

1. Ader C, Schneider R, Seidel K, Etzkorn M, Becker S, Baldus M (2009) Structural rearrangements of membrane proteins probed by water-edited solid-state NMR spectroscopy. J Am Chem Soc 131(1):170–176. doi:10.1021/ja806306e
2. Castellani F, van Rossum B, Diehl A, Schubert M, Rehbein K, Oschkinat H (2002) Structure of a protein determined by solid-state magic-angle-spinning NMR spectroscopy. Nature 420(6911):98–102. doi:10.1038/nature01070
3. Gustavsson M, Verardi R, Mullen DG, Mote KR, Traaseth NJ, Gopinath T, Veglia G (2013) Allosteric regulation of SERCA by phosphorylation-mediated conformational shift of phospholamban. Proc Natl Acad Sci USA 110(43):17338–17343. doi:10.1073/pnas.1303006110
4. Hong M, Zhang Y, Hu F (2012) Membrane protein structure and dynamics from NMR spectroscopy. Annu Rev Phys Chem 63:1–24. doi:10.1146/annurev-physchem-032511-143731
5. Hu F, Luo W, Hong M (2010) Mechanisms of proton conduction and gating in influenza M2 proton channels from solid-state NMR. Science 330(6003):505–508. doi:10.1126/science.1191714
6. Wang S, Ladizhansky V (2014) Recent advances in magic angle spinning solid state NMR of membrane proteins. Prog Nucl Magn Reson Spectrosc 82:1–26. doi:10.1016/j.pnmrs.2014.07.001
7. Zhou HX, Cross TA (2013) Influences of membrane mimetic environments on membrane protein structures. Annu Rev Biophys 42:361–392. doi:10.1146/annurev-biophys-083012-130326
8. Zachariae U, Schneider R, Briones R, Gattin Z, Demers JP, Giller K, Maier E, Zweckstetter M, Griesinger C, Becker S, Benz R, de Groot BL, Lange A (2012) β-barrel mobility underlies closure of the voltage-dependent anion channel. Structure 20(9):1540–1549. doi:10.1016/j.str.2012.06.015
9. Vostrikov VV, Gustavsson M, Gopinath T, Mullen D, Dicke AA, Truong V, Veglia G (2016) Ca^{2+} ATPase conformational transitions in lipid bilayers mapped by site-directed Ethylation and

solid-state NMR. ACS Chem Biol 11(2): 329–334. doi:10.1021/acschembio.5b00953

10. McDermott A (2009) Structure and dynamics of membrane proteins by magic angle spinning solid-state NMR. Annu Rev Biophys 38:385–403. doi:10.1146/annurev.biophys.050708.133719
11. Mainz A, Peschek J, Stavropoulou M, Back KC, Bardiaux B, Asami S, Prade E, Peters C, Weinkauf S, Buchner J, Reif B (2015) The chaperone alphaB-crystallin uses different interfaces to capture an amorphous and an amyloid client. Nat Struct Mol Biol 22(11):898–905. doi:10.1038/nsmb.3108
12. Gor'kov PL, Chekmenev EY, Li C, Cotten M, Buffy JJ, Traaseth NJ, Veglia G, Brey WW (2007) Using low-E resonators to reduce RF heating in biological samples for static solid-state NMR up to 900 MHz. J Magn Reson 185(1):77–93. doi:10.1016/j.jmr.2006.11.008
13. McNeill SA, Gor'kov PL, Shetty K, Brey WW, Long JR (2009) A low-E magic angle spinning probe for biological solid state NMR at 750 MHz. J Magn Reson 197(2):135–144. doi:10.1016/j.jmr.2008.12.008
14. Stringer JA, Bronnimann CE, Mullen CG, Zhou DH, Stellfox SA, Li Y, Williams EH, Rienstra CM (2005) Reduction of RF-induced sample heating with a scroll coil resonator structure for solid-state NMR probes. J Magn Reson 173(1): 40–48. doi:10.1016/j.jmr.2004.11.015
15. Maly T, Debelouchina GT, Bajaj VS, Hu KN, Joo CG, Mak-Jurkauskas ML, Sirigiri JR, van der Wel PC, Herzfeld J, Temkin RJ, Griffin RG (2008) Dynamic nuclear polarization at high magnetic fields. J Chem Phys 128(5):052211. doi:10.1063/1.2833582
16. Wickramasinghe NP, Parthasarathy S, Jones CR, Bhardwaj C, Long F, Kotecha M, Mehboob S, Fung LW, Past J, Samoson A, Ishii Y (2009) Nanomole-scale protein solid-state NMR by breaking intrinsic 1HT1 boundaries. Nat Methods 6(3):215–218. doi:10.1038/nmeth.1300
17. Chevelkov V, Rehbein K, Diehl A, Reif B (2006) Ultrahigh resolution in proton solid-state NMR spectroscopy at high levels of deuteration. Angew Chem Int Ed Engl 45(23):3878–3881. doi:10.1002/anie.200600328
18. Chevelkov V, Xiang S, Giller K, Becker S, Lange A, Reif B (2015) Perspectives for sensitivity enhancement in proton-detected solid-state NMR of highly deuterated proteins by preserving water magnetization. J Biomol NMR 61(2): 151–160. doi:10.1007/s10858-015-9902-2
19. Fu R, Brey WW, Shetty K, Gor'kov P, Saha S, Long JR, Grant SC, Chekmenev EY, Hu J, Gan Z, Sharma M, Zhang F, Logan TM, Bruschweller R, Edison A, Blue A, Dixon IR, Markiewicz WD, Cross TA (2005) Ultra-wide bore 900 MHz high-resolution NMR at the national high magnetic field laboratory. J Magn Reson 177(1):1–8. doi:10.1016/j.jmr.2005.07.013
20. Gopinath T, Veglia G (2012) Dual acquisition magic-angle spinning solid-state NMR-spectroscopy: simultaneous acquisition of multidimensional spectra of biomacromolecules. Angew Chem Int Ed Engl 51(11):2731–2735. doi:10.1002/anie.201108132
21. Gopinath T, Veglia G (2013) Orphan spin operators enable the acquisition of multiple 2D and 3D magic angle spinning solid-state NMR spectra. J Chem Phys 138(18):184201. doi:10.1063/1.4803126
22. Gopinath T, Veglia G (2016) Multiple acquisitions via sequential transfer of orphan spin polarization (MAeSTOSO): how far can we push residual spin polarization in solid-state NMR? J Magn Reson 267:1–8. doi:10.1016/j.jmr.2016.03.001
23. Gopinath T, Veglia G (2016) Orphan spin polarization: a catalyst for high-throughput solid-state NMR spectroscopy of proteins. Annu Rep NMR Spectrosc 89: 103–121
24. Mote KR, Gopinath T, Veglia G (2013) Determination of structural topology of a membrane protein in lipid bilayers using polarization optimized experiments (POE) for static and MAS solid state NMR spectroscopy. J Biomol NMR 57(2):91–102. doi:10.1007/s10858-013-9766-2
25. Pines A, Gibby GM, Waugh JS (1973) Proton-enhanced NMR of dilute spins in solids. J Chem Phys 59:569–590
26. Kupce E, Kay LE, Freeman R (2010) Detecting the "afterglow" of 13C NMR in proteins using multiple receivers. J Am Chem Soc 132(51): 18008–18011. doi:10.1021/ja1080025
27. Bellstedt P, Herbst C, Hafner S, Leppert J, Gorlach M, Ramachandran R (2012) Solid state NMR of proteins at high MAS frequencies: symmetry-based mixing and simultaneous acquisition of chemical shift correlation spectra. J Biomol NMR 54(4):325–335. doi:10.1007/s10858-012-9680-z
28. Banigan JR, Traaseth NJ (2012) Utilizing afterglow magnetization from cross-polarization magic-angle-spinning solid-state NMR spectroscopy to obtain simultaneous heteronuclear multidimensional spectra. J Phys Chem B 116(24): 7138–7144. doi:10.1021/jp303269m
29. Andreas LB, Le Marchand T, Jaudzems K, Pintacuda G (2015) High-resolution proton-detected NMR of proteins at very fast MAS. J

Magn Reson 253:36–49. doi:10.1016/j.jmr.2015.01.003

30. Paulson EK, Morcombe CR, Gaponenko V, Dancheck B, Byrd RA, Zilm KW (2003) Sensitive high resolution inverse detection NMR spectroscopy of proteins in the solid state. J Am Chem Soc 125(51):15831–15836. doi:10.1021/ja037315+
31. Buck B, Zamoon J, Kirby TL, DeSilva TM, Karim C, Thomas D, Veglia G (2003) Overexpression, purification, and characterization of recombinant Ca-ATPase regulators for high-resolution solution and solid-state NMR studies. Protein Expr Purif 30(2):253–261
32. Bennett AE, Rienstra CM, Auger M, Lakshmi KV, Griffin RG (1995) Heteronuclear decoupling in rotating solids. J Chem Phys 103(16): 6951–6958. doi:10.1063/1.470372
33. Hartmann SR, Hahn EL (1962) Nuclear double resonance in the rotating frame. Phys Rev 128(5):2042–2053
34. Detken A, Hardy EH, Ernst M, Kainosho M, Kawakami T, Aimoto S, Meier BH (2001) Methods for sequential resonance assignment in solid, uniformly ^{13}C, ^{15}N labelled peptides: quantification and application to antamanide. J Biomol NMR 20(3):203–221.
35. Franks WT, Kloepper KD, Wylie BJ, Rienstra CM (2007) Four-dimensional heteronuclear correlation experiments for chemical shift assignment of solid proteins. J Biomol NMR 39(2):107–131. doi:10.1007/s10858-007-9179-1
36. Verel R, Ernst M, Meier BH (2001) Adiabatic dipolar recoupling in solid-state NMR: the DREAM scheme. J Magn Reson 150(1): 81–99. doi:10.1006/jmre.2001.2310
37. Takegoshi K, Nakamura S, Terao T (2001) ^{13}C-^{1}H dipolar-assisted rotational resonance in magic-angle spinning NMR. Chem Phys Lett 344(5–6):631–637. doi:10.1016/S0009-2614(01)00791-6
38. Delaglio F, Grzesiek S, Vuister GW, Zhu G, Pfeifer J, Bax A (1995) NMRPipe: a multidimensional spectral processing system based on UNIX pipes. J Biomol NMR 6(3):277–293



http://www.springer.com/978-1-4939-7385-9

Protein NMR
Methods and Protocols
Ghose, R. (Ed.)
2018, XIII, 446 p. 62 illus. in color., Hardcover
ISBN: 978-1-4939-7385-9
A product of Humana Press